Conduction mechanisms during the growth of Pd thin films: Experiment and model

Stefan Wagner and Astrid Pundt
Institute for Materials Physics, University of Göttingen, D-37077 Göttingen, Germany
(Received 9 May 2008; revised manuscript received 8 July 2008; published 30 October 2008)

The conduction mechanisms in different growth stages of Pd thin films are investigated in detail. Special attention is paid to the transition regions between the different stages of film growth and the dominant conduction mechanisms. Mechanisms of thermally activated tunneling, percolation conduction, and continuous film conduction are considered and a consistent set of model parameters is deduced. This is done by also varying the substrates. Activation energies of tunneling on the order of 50 meV, percolation thresholds $p_c = 0.70 \pm 0.01$, and conduction exponents $\mu = 2.43 \pm 0.12$ were achieved. The physical meaning of the model parameters is discussed and connected mechanisms are proposed. The minimal film thicknesses of continuous RT-sputtered Pd films were found to be on the order of 1.5 nm.

DOI: 10.1103/PhysRevB.78.155131 PACS number(s): 73.50.−h

I. INTRODUCTION

Within the increasing demands in miniaturization in various fields of research and technological applications, the question on the mechanisms of electrical conduction in nanosized metal systems is of central importance. The number of different conduction models proposed in literature is as manifold as the number of different systems investigated, spanning both classical and quantum-mechanical models.[1–10] A fundamental problem regarding this topic results from the coappearance of different mechanisms simultaneously affecting the electrical conductance, making the investigations complex. Often conflicting results appear when single theories are exclusively applied.

Metal films on insulating substrates often start growing from small isolated islands, which interconnect and percolate at a certain state of growth, leading to the formation of a continuous network structure and finally forming a compact layer. Accompanying these different stages of growth, different conduction mechanisms appear, subsequently gaining and loosing importance for the total film conductivity. These mechanisms may be classified as tunneling conduction, percolation conduction, and continuous film conduction.[9,11,12] Nevertheless, in literature researchers often focus on one stage of film growth, investigating the predominant conduction mechanism[5,6,13–19] or they hint at the existence of other mechanisms without further elaboration.[12,20] Compiling these results, often inconsistencies regarding the model parameters appear as, for example, a meta-analysis of the data given by Kazmerski and Racine[21] yields dielectric constants smaller than 1. The aim of the present work, therefore, is to attempt to establish a consistent description of the conduction mechanisms in all stages of a continuously growing Pd film, especially regarding the transition regions, and determining as well effects that have been missed up to now.

From a practical point of view, the questions regarded in this work are of special interest in resistance based sensor technologies. There, nanosized systems offer unique properties such as large surface areas and short switching times. Dankert and Pundt[22] and Lith *et al.*[23] established the idea of induced percolation of discontinuous Pd films, resulting from the volume increase in Pd clusters during hydrogen absorption. For the interpretation of the related decrease in the electrical resistance, detailed knowledge on the resistance evolution and related mechanisms is needed. Thus, the results of the present work might help us to optimize the sensor properties of such systems as well.

II. THEORY: DIFFERENT CONDUCTION REGIMES

The conduction mechanisms in thin metal films strongly depend on the film morphology in the different stages of growth, which is ruled by the kinetics and the thermodynamics of the metal atoms on the substrate surface.[24] Metallic films mostly start to grow as statistically distributed and isolated metal islands.[25] As illustrated in Fig. 1, during further deposition these islands increase in size, while their distances decrease, until the islands start to coalesce to form larger but still isolated islands. Reaching a critical value of the island radius, remarkable changes in the island growth behavior occur.[26] Now, islands do not fully coalesce any longer but start to form elongated isolated clusters, which with the further supply of matter start interconnecting and forming a network structure. Reaching the percolation threshold, a supercluster occurs, spanning the whole substrate. This spanning cluster finally densifies, leading to the formation of a continuous metal film. From this, metallic film growth on insulating substrates can be summarized to run through the three distinguished states of isolated islands, the physical contact between the islands and the formation of a network structure (percolation), and finally the formation of a continuous film.

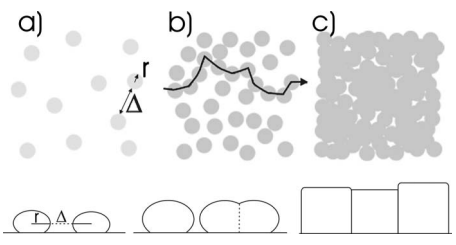

FIG. 1. The three stages of thin-film growth: Isolated islands, percolating network structure, and continuous film. At the percolation threshold continuous conductions paths occur.

Therefore, three large groups of conduction mechanisms exist, supporting the electrical conductivity in the distinguished states of growth. For the state of isolated islands, quantum-mechanical mechanisms dominate. The formation of a network structure leads to percolation conduction, and in the final state of a continuous film, mechanisms of Fuchs-Sondheimer conduction occur. Of course these mechanisms are not perfectly separated from each other; they are expected to evolve and overlap in transition regions between the different states of growth. The gain and loss of their importance for the total conductivity make the analysis of the resistance progression of a growing film quite difficult.

A. Conduction between isolated islands

The electrical transport in discontinuous metal films in the state of isolated islands is a matter of dispute up to this day, as here different possible conduction mechanisms occur simultaneously[9,17,27] and it is not clarified which model is the most proper one. All models have to explain the transport of electrons over the gap between the islands, but they differ in the way the electrons are moving. On one hand, mechanisms of quantum-mechanical tunneling occur, such as thermally activated tunneling, vacuum tunneling between allowed states, and substrate assisted tunneling. On the other hand, mechanisms of thermionic emission are discussed.

A basic quantity of the electric transport in discontinuous metal films is the appearance of a Coulomb blockade, resulting from the electron transition between two initially neutral islands, leading to the formation of a positively and a negatively charged island. Therefore, electron transport in discontinuous films needs an activation energy E_a, supplying the electrostatic energy of the resulting electric field. The assumption of an activated charge transfer thereby arises from the observation of a negative temperature coefficient of resistance (TCR) α of discontinuous films,[28] $\alpha := (1/R)(dR/dT)$, leading to an activated conduction with the resistance $R=R_0 \exp(E_a/k_BT)$. Now the challenge of the conduction models is the calculation of the prefactor R_0 and the activation energy E_a. Until the early 1960s, the electronic properties of discontinuous films were widely described in terms of thermionic emission, while nowadays the focus lies on models for an activated tunneling mechanism.[29] Hill[10] and Ostadal and Hill[16] pointed out that thermionic emission becomes the dominant charge transport mechanism for island separations larger than 10 nm.

Today the widely used models for the description of electrical transport between isolated islands on an insulating substrate are based on the model of Neugebauer and Webb.[30] In a two-step process, in this model first the number of charged islands in the arrangement of all islands is determined, and from this in the second step the film resistance is calculated from the electron current between charged and formerly uncharged islands. This leads to the resistivity $\rho \sim (r/e^2\Delta^2)(1/D)\exp(E_a/k_BT)$, depending on the electron charge e, the temperature T, the island separation Δ, the island radius r, and the transmission coefficient D of tunneling. In the simplest case the resistivity turns out to be independent of external electrical fields supplied between the islands, and in the model Neugebauer and Webb[30] consider the metal islands as perfectly isolated from each other. As Hill[10] pointed out, these assumptions are questionable, as an external field shifts the relative positions of the Fermi levels of adjacent islands and this affects the tunneling mechanism. Additionally, as even a low electron affinity of the substrate will lower the energy barrier between the islands, electron transfer via the substrate will be energetically favorable compared to vacuum tunneling. Taking this into account, Hill[10] calculated the transmission coefficient and from this the resistivity of the discontinuous film under consideration of the height of the tunneling barrier and an external field F, finding in the practical case $E_a > k_BT$ that

$$\rho_{\mathrm{Hill}}(V,T) = \frac{h^3B^2}{8\pi m_e e}\sinh^{-1}\left(\frac{eV}{k_BT}\right)\frac{\sin(\pi Bk_BT)}{\pi Bk_BT} \times \exp(A\sqrt{\bar{\phi}})\exp\left(\frac{E_a}{k_BT}\right).$$

Here $B=A/2\sqrt{\bar{\phi}}$ and $A=(4\pi/h)\sqrt{2m_e}\Delta$, with the effective barrier height $\bar{\phi}$ and the mass m_e of the tunneling electron. $V=F(2r+\Delta)$ with the average field F over the sample, and h is Planck's constant. The result of Hill[10] is valid for coplanar electrodes, not taking into account the curvature of the islands' surfaces. Taking on the idea of Kazmerski and Racine[21] to combine the results of Hill[10] and Neugebauer and Webb,[30] which account for the cross section of the tunneling area, we gain the best approximation of the resistivity of a discontinuous film,

$$\rho(V,T) \sim \frac{r}{e^2\Delta^2}\rho_{\mathrm{Hill}}(V,T), \tag{1}$$

which is slightly different from the equation of Kazmerski and Racine.[21]

This equation is the basis of the analysis in the experimental part of this work. With Eq. (1) the activation energy E_a can be derived, which, again, contains material parameters that need to be consistent with literature data. This comparison is nowadays often left aside. Since this leads to conflicting results, it will be regarded more intensely here.

Two different models are discussed to calculate the activation energy E_a. Many authors[10,16] consider the pair of islands taking part in the charge transfer isolated from the other islands (Fig. 1) and calculate the electrostatic energy E_{es} of two spherical electrodes with radius r and distance Δ, setting

$$E_a := E_{\mathrm{es}} = \frac{e^2}{4\pi\varepsilon_0\varepsilon_r}\left(\frac{1}{r} - \frac{1}{2r+\Delta}\right). \tag{2}$$

Here ε_0 is the electric-field constant and ε_r is the dielectric constant of the system. The calculation of the activation energy in this picture of pair charges is problematic, as it does not take into account possible polarization effects on surrounding metal islands, complicating the calculation of the electric field.

Alternatively, Abeles *et al.*[31] developed a model for the activation energy of tunneling in cermets, which might be applicable for discontinuous films as well. In this model, a

charged spherical island and its adjacent islands are considered as a spherical capacitor with the radius $r+\Delta$ and the electrostatic energy

$$E_a = \frac{e^2}{8\pi\varepsilon_0\varepsilon_r}\left(\frac{1}{r} - \frac{1}{r+\Delta}\right). \tag{3}$$

The dielectric constant ε_r in both models contains substrate and vacuum contributions and, therefore, is set as a linear combination of the dielectric constants of the vacuum, $\varepsilon_{\mathrm{vac}}=1$, and the substrate,[5]

$$\varepsilon_r = m\varepsilon_{\mathrm{vac}} + (1-m)\varepsilon_{\mathrm{sub}}, \quad \text{with} \quad 0 < m < 1. \tag{4}$$

It remains as a fitting result via m, which weights the vacuum or substrate assisted tunneling.

Usually, the shapes of the growth islands themselves are not spheres but closer to prolate ellipsoids (compare Fig. 1). With the shape of the islands their capacity changes, leading to deviations in the activation energy. Hill[10] discussed this problem for special cases, but, more recently, it is often neglected.[5,16] Following Jeans,[32] the capacity C of an ellipsoidal growth island with half axes a, b, and c is calculated as

$$C = 4\pi\varepsilon_0\varepsilon_r\left[2/\int_0^\infty \frac{d\lambda}{\sqrt{(a^2+\lambda)(b^2+\lambda)(c^2+\lambda)}}\right], \tag{5}$$

which is evaluated in this work. For the determination of the activation energy of charge transfer, it is useful to compare the capacity C of the islands to that of a sphere, $\bar{C}$, of equivalent lateral radius $\bar{r}=\sqrt[2]{ab}$, giving a new prefactor $K=4C/\bar{C}$ in Eq. (2). This results in the general expression

$$E_a = \frac{e^2}{K\pi\varepsilon_0\varepsilon_r}\left(\frac{1}{\bar{r}} - \frac{1}{2\bar{r}+\Delta}\right) \tag{6}$$

in the pair-charge model, which will be the favored one in this paper, as it fits the experimental data better than the spherical capacitor model of Eq. (3).

The combination of Eqs. (1) and (6) leads to the possibility of a direct determination of the dielectric constant ε_r of the Pd-substrate system, as the resistance R of a Pd film with length L, width b, and thickness d is

$$R \sim M\frac{\bar{r}}{d\Delta}\sin\left(\frac{2\pi^2 k_B T}{h}\sqrt{\frac{2m_e}{\bar{\phi}}}\Delta\right)\exp\left[\frac{4\pi}{h}\sqrt{2m_e\bar{\phi}}\Delta + \frac{e^2}{K\pi\varepsilon_0\varepsilon_r k_B T}\left(\frac{1}{\bar{r}} - \frac{1}{2\bar{r}+\Delta}\right)\right], \tag{7}$$

with

$$M = \frac{h^2}{4\pi m_e e^3 k_B T}\frac{L}{b}\sinh^{-1}\left(\frac{eV}{k_B T}\right)\sqrt{\frac{2m_e}{\bar{\phi}}},$$

which is the final equation for the evaluation of the resistance curves of growing thin Pd films in the tunneling region. Apart from ε_r in Eq. (7), the effective tunneling barrier height $\bar{\phi}$, the mass m_e of the tunneling electron, and the geometry factor $K=K(a,b,c)$ are present, which have to be determined first.

The calculation of the effective tunneling barrier height $\bar{\phi}$ is difficult as it requires exact knowledge of the geometry of the barrier.[33] Alternatively, Hill[10] calculated the barrier height for Au clusters on glass from the temperature dependence of the resistance, giving $\phi_{\text{Au-glass}}\approx 0.56$ eV and $m_e=0.41m_0$, with the electron rest mass m_0. As Au and Pd exhibit comparable work functions ($\chi_{\mathrm{Au}}=4.46$ eV and $\chi_{\mathrm{Pd}}=4.45$ eV), these results will be stressed for the Pd thin films as well, setting $\bar{\phi}_{\text{Pd-sa,gl}}\approx 0.56$ eV and $m_e=0.41m_0$ for glass and the sapphire substrates. In case of silicon substrates, a rough approximation of the barrier height is given by the difference between the work function χ_{Pd} of Pd and the electron affinity $\psi_{\mathrm{Si}}=4.05$ eV of silicon.[34] Taking into account the thin native oxide layer, it is finally assumed that $\chi_{\text{Pd-Si(O}_2\text{)}}\approx 0.45$ eV and $m_e=0.41m_0$.

Further, the nature of the activation energy itself has to be regarded, which is also not taken into account in recent literature. Complex models regarding different contributions to the activation energy have been proposed.[29,35,36] These models have the disadvantage that they cannot be directly fitted to the measured data, as will be explained later on. However, the models will be figured out in the following and the results gained in this work will be discussed with respect to them.

In the pair-charge model the activation energy is calculated for the charge transfer between initially neutral islands and thereby is directly linked to the charge transfer. In their original model, Neugebauer and Webb[30] otherwise considered the process of a thermally activated charge creation and a subsequent nonactivated charge transport. Here it is left out of consideration that the charge flipping process itself actually is too fast to allow electrostatic relaxation of the island system, leading to polarization effects. Therefore, as Dryer *et al.*[36] pointed out, in principle the total activation energy is a sum of the activation energy of charge creation and an overcoming of the polarization effects. Moreover, depending on the process, ε_r is given by the high-frequency values $\varepsilon_r^{\mathrm{opt}}$ or the low-frequency values $\varepsilon_r^{\mathrm{acus}}$. Leaver[35] and Dryer *et al.*[36] calculated the activation energy of charge transfer E_a^t referring to the high-frequency and the static charging components as

$$E_a^t = \frac{e^2}{4\pi\varepsilon_0}\left(\frac{1}{\varepsilon_r^{\mathrm{opt}}} - \frac{1}{\varepsilon_r^{\mathrm{acus}}}\right)\left(\frac{1}{r} - \frac{1}{2r+\Delta}\right). \tag{8}$$

The activation energy of charge creation E_a^e is given as $E_a^e=(e^2/8\pi\varepsilon_0\varepsilon_r^{\mathrm{acus}})(1/r)$. Furthermore, Leaver[35] pointed out that in case $E_a\approx k_B T$, the number of charged islands is so high that they are not electrically independent, resulting in deviations from the Boltzmann distribution of their number. For the resulting activation energy of charge creation, Leaver gave[35]

$$E_a^{e'} = \frac{e^2}{4\pi\varepsilon_0\varepsilon_r^{\mathrm{acus}}}\left(\frac{1}{r} - \frac{\alpha}{R}\right) = E_a^e\left(1 - \frac{\alpha r}{R}\right), \tag{9}$$

with an effective distance R of the charge carriers and the Madelung constant α of the film geometry.

As it turns out here, the parameters set in the models of Neugebauer and Webb[30] and Hill[10] in Eqs. (1) and (7) are

pure model parameters. Their physical meaning will be discussed reverting to the model of Dryer *et al.*[36] and Leaver.[35]

B. Percolation conduction

When the morphology of the growing discontinuous film reaches the second state of growth, forming elongated and interconnected structures, the contribution of the tunneling mechanism will recede behind a conduction mechanism linked to conduction paths in the network structure. This regime is described by the percolation theory,[37] applying either lattice percolation models or more confined models that take the random film dispersion into account.[38] In these models, the surface fraction p of the system, covered by the film, controls the physical properties.[39] For $p<p_c$ only local clusters are present; for $p>p_c$ spanning clusters linking both sample borders cover the surface. At the percolation threshold p_c, the surface coverage p results in the first spanning cluster. The percolation transition is a phase transition of second order, as the physical and the geometrical properties of the percolating system diverge or converge continuously at p_c with power laws of the quantity $|p-p_c|$. Another basic property of percolating systems is their self-similarity on length scales $r<\xi$ with the correlation length ξ, diverging at p_c but finite below and above p_c, $\xi \sim |p-p_c|^{-\upsilon}$.[37]

The existence of fractal geometry, which is required to apply percolation theory to the growth of thin films, was confirmed by Kapitulnik and Deutscher[40] for growing Pb thin films on amorphous Ge substrates. Thus, the resistance of a growing metal film near the percolation threshold for $p>p_c$ is expected to follow[39]

$$R \sim (p-p_c)^{-\mu}, \tag{10}$$

with the conduction exponent μ mainly depending on the dimensionality [$\mu^{2D}=1.3$,[14] $p_c^{2D}=0.688$,[41] $\mu^{3D}=1.4\pm0.1$,[42] and $p_c^{3D}=0.29$ [39]]. Regarding their geometrical properties, random percolating systems belong to universality classes, distinguished based on their geometrical dimensions only. But, regarding the physical properties, this classification does not hold in general, as the model parameters may vary with the specific properties of the percolating system.[37]

C. Continuous film conduction

With proceeding percolation, the film morphology becomes more and more continuous, raising the importance of electron scattering at the microstructure of the film. Additional to the contributions subsumed in the Matthiessen rule, scattering will occur at the film surface, grain boundaries, and the surface roughness, as their dimensions are on the order of the mean free path l_0 of the scattered electrons, leading to a significantly increased film resistance compared to that of bulk.[9] Beyond the models of Sondheimer[43] and Rahman[44] for surface scattering, of Mayadas and Shatzkes[45] and Tellier *et al.*[46] for the contribution of grain boundaries, and of Angadi[9] for the roughness scattering, the model of Finzel and Wissmann[47] is of practical importance, as it subsumes the formerly mentioned single contributions. For polycrystalline metal films of thickness d with a Gaussian distribution of the surface roughness and meander morphology, it is concluded[47] that

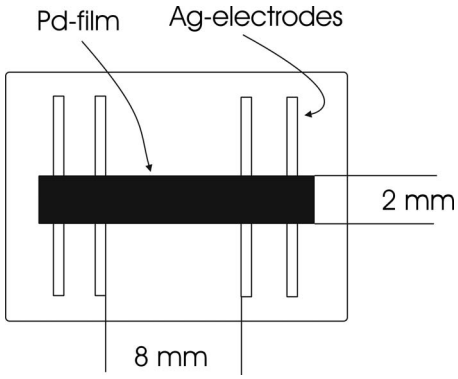

FIG. 2. The Pd films have been sputtered perpendicular to four parallel Ag electrodes on the substrate, permitting *in situ* four-point probe of the resistance of the growing film.

$$\rho = \rho_{\mathrm{Ohm}} + \rho_{\mathrm{GB}} + \rho_{\mathrm{rough}} = \rho_0\left(1 + Z\Lambda\frac{l_0}{d} + Z\Lambda\Theta^2\frac{l_0}{d^3}\right). \tag{11}$$

Here Z represents the number of scattering centers with the effective scattering cross section Λ, and Θ is the amplitude of the roughness distribution. In this model, surface scattering is much less important than grain-boundary scattering, which was shown experimentally by Finzel and Wissmann[47] for thin polycrystalline films.

III. APPLIED METHODS AND SAMPLE PREPARATION

Discontinuous Pd films have been prepared by cathode beam sputtering using a low sputtering rate. All films have been sputtered at room temperature in an UHV chamber with a base pressure of 10^{-8} Pa and an Ar gas (6N quality) pressure of 10^{-2} Pa during deposition. The low sputter rate $\tau < 0.2$ nm/min was monitored by a quartz-crystal oscillator. It is similar to the conventional deposition rates during thermal evaporation. During sputtering, the resistance of the growing films was measured *in situ* by a four-point probe. Therefore, prior to sputtering the metal films, four parallel Ag electrodes with the dimensions $1.0\ \mathrm{cm}\times 0.1\ \mathrm{cm}\times 100$ nm have been sputtered onto the substrates through a mask. The sample geometry is shown in Fig. 2.

These electrodes were contacted with cantilever contacts in the sample holder for the Pd-film deposition. The Pd film was deposited perpendicular to the electrodes through a slit with the dimensions $1.3\times 0.2\ \mathrm{cm}^2$. The measuring four-point probe voltage was set automatically in the range of 1–5 V by a Keithley 199. To prevent local heating effects in the percolation paths of the growing thin film, the measuring currents have been limited to $I\leq 10\ \mu$A by applying an additional resistor in series with the sample. The substrates' sizes were $1.6\times 1.3\ \mathrm{cm}^2$.

Different substrates with high specific resistances ($>10^{13}\ \Omega$ cm) were chosen to allow the determination of different substrate properties onto the Pd-film growth. Slide

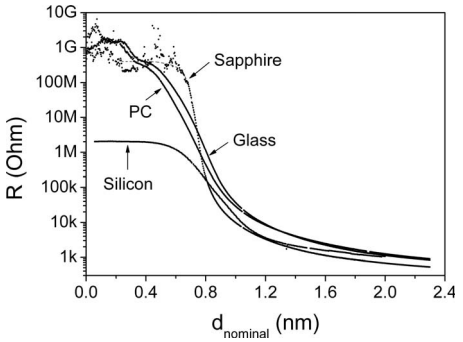

FIG. 3. Representative resistance developments of growing Pd films on different substrates, exhibiting similar behaviors in general but differing in detail. The overall resistance decrease amounts up to six orders of magnitude.

glass, sapphire ($11\bar{2}0$ orientation), and polycarbonate have been used. Additionally, low resistance silicon (100) substrates with their native oxide layer have been applied in order to permit scanning tunneling microscopy (STM) measurements. During the resistance measurements, at the electrical contacts in the sputter chamber a parallel resistance on the order of 20 MΩ occurred after a short operating time, which was corrected by applying $1/R_{\mathrm{Pd}}=1/R_{\mathrm{measured}}-1/R_{\mathrm{parallel}}$.

Information on the film morphology, e.g., island size, island separation, and surface coverage, was gained by performing scanning tunneling microscopy (UHV-micro-STM; Omicron) and scanning electron microscopy (SEM) (LEO-SUPRA 35). Image series on Pd films with different nominal thicknesses were taken. The surface coverage has been determined by applying the image analysis software IMAGEJ 1.33©.

IV. EXPERIMENTAL RESULTS

Representative resistance data depending on the nominal thickness of Pd films are summarized in Fig. 3. It gives the results for films grown on glass, sapphire, polycarbonate, and silicon on a logarithmic scale. The resistance curves exhibit similar behaviors but they are different in detail. In the initial state of growth, the film resistances stay nearly constant until they start decreasing at nominal film thicknesses between 0.5 and 0.7 nm, and then drop down by almost 6 orders of magnitude. Due to the substrate conductivity of silicon, the resistance drop amounts to about 3 orders of magnitude. Thereafter, the resistance evolution becomes less steep at about 1 nm film thickness again, leading to a slow decrease during further film growth. But, especially for glass and polycarbonate (PC) in the earliest stages of growth, deviations from this general behavior occur, expressed as a smooth initial increase in the resistance, which is followed by a steep decay and a subsequent smoother propagation, before the large drop occurs. Therefore, substrate dependent differences in the resistance propagations are present, presumably also resulting from the different film morphologies. As the film morphologies are input parameters for the evaluation of the film resistances, they will be described first.

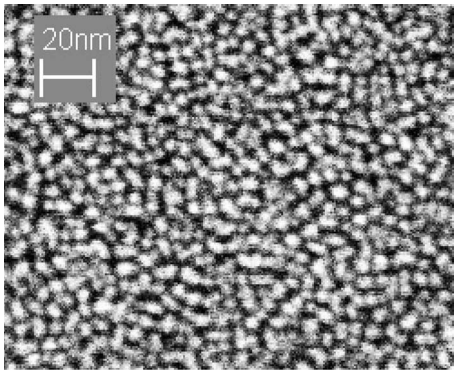

FIG. 4. SEM image of Pd on silicon substrate. The nominal film thickness is 0.53 nm.

A. Film morphologies

The SEM images confirm the islandlike initial film morphology. In Fig. 4 a typical SEM image of Pd on silicon is shown. The surface coverage p, the mean island radii $\bar{r}$, and mean island distances Δ were determined and gave qualitatively similar results for the evolution of the mean island distances for Pd on silicon, glass, and sapphire, but exhibited clearly different mean island sizes. The mean island size is smallest on sapphire and largest on glass. Connected to this are tendencies of a rapid island size growth on sapphire, while the Pd islands on glass are growing slower with increasing film thickness. The resulting fitted dependencies from the nominal film thicknesses are given in Table I. In the investigated film thickness interval $d>0.2$ nm, the mean radii depend linearly and the distances quadratically on the film thickness. For smaller thicknesses different parameter dependencies might occur.

The evolution of the surface coverages p interestingly does not exhibit significant differences between the analyzed substrates, as shown in Fig. 5. Obviously the surface coverage initially increases rapidly with increasing film thickness, but the increase ebbs above $d_{\mathrm{nom}}\approx 0.8$ nm. In the initial stage of film growth up to $p=0.65$, the surface coverage has been fitted by the power law $p(d)=Cd_{\mathrm{nom}}^{k}$, with $C=0.83(2)$ and $k=0.56(2)$, explainable by ellipsoidal island growth[48] and valid for Pd on silicon, sapphire, and glass.

Strong charging effects impede SEM morphology studies of Pd films grown on PC, while for glass and sapphire it was possible to overcome charging effects using silver paint. But, as the surface coverages of Pd for the other substrates are quite similar, it is assumed to be the same for the PC substrate as well.

The geometry factor K of Eq. (6) for Pd films grown on silicon substrates was derived by analyzing STM images. As shown in Fig. 6, horizontal and vertical ellipses have been fitted to about 20 growth islands, giving the mean half axes a, b, and c. The capacity of the growth islands was calculated from Eq. (5), resulting in $K(a,b,c)_{\mathrm{Si}}=2.87$. The K factors for Pd on glass and sapphire have been determined by examining the mean island radius $\bar{r}$ from SEM images and by assuming that the height of the growth islands resembles that of Pd on silicon. This is based on the finding of similar surface coverages, which means that the same Pd-film vol-

TABLE I. Tunneling regime: Pd-film morphologies on silicon, sapphire, and glass as well as model parameters referring to the model of Neugebauer and Webb (Ref. 30) and Hill (Ref. 10). Section 1: Mean island sizes and island distances as functions of the nominal film thickness. Section 2: Mean island sizes and resulting geometry factors K for Pd films with $d_{\mathrm{nom}}=0,70$ nm. Section 3: Determined dielectric constants ε_r and upper limits of the tunneling regions. Section 4: Substrate dielectricities $\varepsilon_{\mathrm{sub}}$ and calculated mixing parameters $1-m$, representing the contribution of substrate assisted tunneling to the tunneling mechanism.

	Substrate/Quantity	Silicon	Sapphire	Glass
1	Mean island size $\bar{r}$ (nm)	$1.98(26)+1.14(1.06)d$	$1.37(46)+1.73(48)d$	$2.63(92)+0.96(98)d$
	Mean island distances Δ (nm)	$3.60-6.05d+4.16d^2$	$3.43-3.58d+1.52d^2$	$4.68-4.52d+1.37d^2$
2	$\bar{r}$ (nm)	2.78	2.58	3.30
	K	2.87	3.07	2.46
3	d_{tunnel} (nm)	<0.74	<0.68	<0.69
	p_{tunnel}	<0.69	<0.67	<0.68
	$g(10^{-9}\ \mathrm{V^2\,s^2/kg\,m})$	7.31 ± 1.89	9.64 ± 0.67	9.49 ± 0.66
	ε_r	10.6 ± 2.5	7.53 ± 0.53	9.18 ± 0.64
4	$\varepsilon_{\mathrm{sub}}$	3.8–11.8	9.3–11.5	4.6–10
	$1-m$	1–0.89	0.79–0.62	1–0.91

ume covers the same surface area fraction, while the total number of growth islands is different. The K factors have been calculated for a nominal film thickness of $d_{\mathrm{nom}}=0.7$ nm in comparison to K_{Si}. The results for K and the mean lateral Pd island radius $\bar{r}$ for the different substrates are summarized in Table I. It can be seen that the mean Pd island radius is largest for Pd on glass, while it is lowest on sapphire, resulting in the largest K value for Pd on sapphire and the smallest K value for Pd on glass. For the calculation of K, the assumption has been made that it is constant during film growth. Obviously this is a rough approximation, as during growth the ellipticity of the islands slightly increases.

In the following the resistance curves of the growing Pd films will be analyzed in terms of the supposed conduction mechanisms. Special attention will be paid on the growth states where the conduction mechanisms superimpose each other, resulting in constraints for the applicability of the single models.

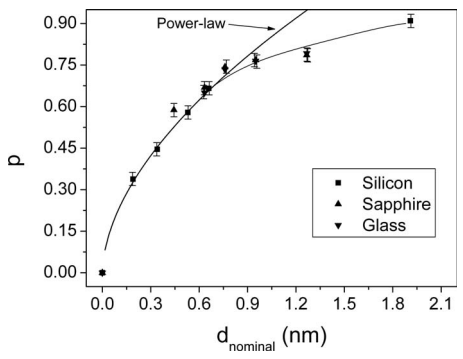

FIG. 5. Surface coverage p of Pd films on silicon, glass, and sapphire substrates. The evolution of p with increasing nominal film thicknesses does not show significant differences between the different investigated substrates. It follows a power-law dependence on d in the initial stages of growth and later on its growth rate decreases.

B. Conduction between isolated islands

Following Eq. (7), with the knowledge of the geometry factor K, the mean barrier height $\bar{\phi}$, and the electron mass m_e, the dielectric constants ε_r of the Pd-substrate systems can be determined by plotting the normalized resistance $R' := R/\Psi$ in logarithmic scale over

$$\frac{1}{\bar{r}}-\frac{1}{2\bar{r}+\Delta},$$

with

$$\Psi = M\frac{\bar{r}}{d\Delta}\sin(\pi Bk_BT)\exp(A\sqrt{\bar{\phi}}).$$

In Fig. 7 the resulting plot for Pd on glass is shown as an example. If the supposed model holds for the initial stages of Pd-film growth, a straight line of the resistance propagation from small film thicknesses (on the right side) to larger film thicknesses (on the left side) is expected. As can be seen in the figure, this relation holds only for a narrow region of film thickness until deviations from the expected behavior occur.

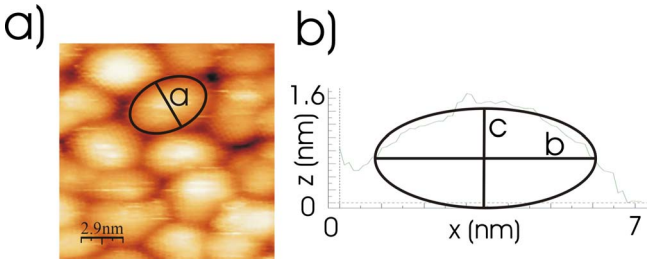

FIG. 6. (Color online) Definition of the ellipsoid half axes of Pd growth islands on silicon. Horizontal (a) and vertical (b) ellipses are fitted to certain growth islands, giving a, b, and c. In average $a=(2.13\pm0.74)$ nm, $b=(1.88\pm0.31)$ nm, and $c=(0.41\pm0.08)$ nm. From this, the capacity of the growth islands can be calculated

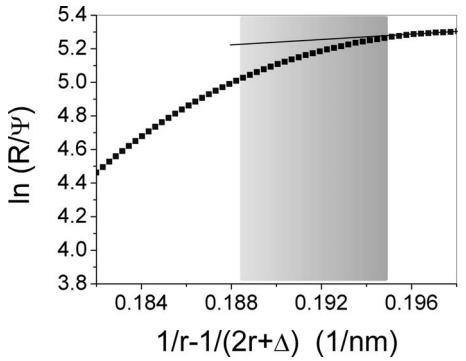

FIG. 7. For the determination of the dielectric constant of the Pd-glass system, the normalized resistance (see text) is plotted over $1/\bar{r}-1/(2\bar{r}+\Delta)$. The slope of the resulting curve in the right half of the figure is a measure for ε_r, while for smaller arguments differences from the expected resistance behavior occur, ascribed to the onset of percolation.

As will be shown below, these deviations can be interpreted based on the appearance of percolation conduction, which interferes with the tunneling resistance. In Fig. 7 the transition region is slightly shaded.

The slope g of the tangent line gives the dielectric constant ε_r of the Pd-substrate system, with $g=(e^2/K\pi\varepsilon_0 k_B T)(1/\varepsilon_r)$. The dielectric constants, calculated for $T=300$ K and the centers d_{tunnel} (or p_{tunnel}, as determined from Fig. 5) of the transition region are summarized in Table I.

Considering the dielectric constant ε_r as constant during film growth, the activation energies of tunneling, $E_a=gk_BT[(1/\bar{r})-1/(2\bar{r}+\Delta)]$, have been calculated and plotted in Fig. 8. For all substrates the activation energies are on the order of 50–100 meV and thereby comparable to theoretical expectations.[10] They slightly decay when the film thickness increases, while this effect is strongest for Pd films on sapphire. The choice of the tangent line in Fig. 7 seems to be arbitrary to some extent. As this problem cannot be solved with the present data evaluation method, independent determinations of the activation energies E_a for Pd films in certain growth states have been performed by thermal heating measurements. These measurements confirm the values determined here (see Fig. 9) and therefore justify the choice of the tangent lines.

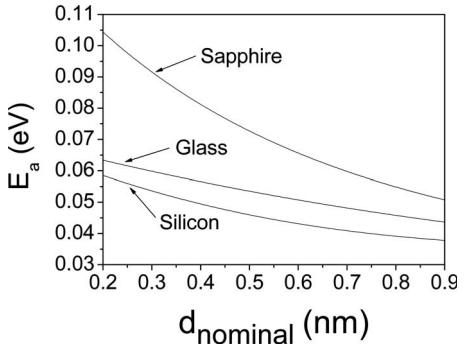

FIG. 8. Activation energies of tunneling in discontinuous Pd films on silicon, glass, and sapphire, calculated in the model of Neugebauer and Webb (Ref. 30) and Hill (Ref. 10).

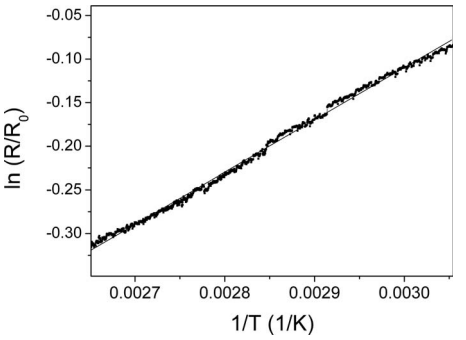

FIG. 9. Temperature dependent resistance of Pd on glass with $R_0=177$ MΩ. The temperature dependent analysis of the resistance of Pd films with a certain thickness gives an independent possibility of confirming the activation energies E_a of tunneling determined from the resistance development of growing films. The activation energy results from the slope $\bar{g}$ of the resistance in the resulting Arrhenius plot. From $\bar{g}=d\ln(R/R_0)/d(1/T)$ and $R(T)=R_0\exp(E_a/k_BT)$, it follows that $E_a=\bar{g}k_B$, resulting in activation energies comparable to those determined from the resistance evolution of growing Pd films. It is $\bar{g}=(597.8\pm0.9)$ K.

From Eq. (4) the substrate contribution to the tunneling mechanism can be calculated assuming the dielectric constants ε_{sub} to be those of the pure substrates. ε_{sub} values taken from literature and the resulting mixing parameters $1-m$ are also given in Table I. For clarity, following the model assumptions of Neugebauer and Webb[30] and Hill,[10] the static values are applied. The physical meaning of the resulting parameters will be discussed later on in terms of the model of Dryer *et al.*[36] and Leaver.[35] Regarding the thin natural oxide layer, for the silicon substrate a dielectric constant between the values for pure silicon and silicon oxide has been assumed. As the oxide layer thickness is on the order of only 1 nm, the effective substrate dielectricity cannot be estimated to be that of pure silicon oxide from first principles.

C. Percolation conduction

In the percolation regime with the percolation threshold p_c, the expected power-law dependence $R\sim(p-p_c)^{-\mu}$ of Eq. (10) has to fit the measured resistance data. But it is not possible to fit the expected power-law dependence to the total percolation region of conduction. As shown in the last paragraph, it has to be taken into account that the percolation conduction is interfered with by a receding tunneling conduction, masking the percolation threshold and modifying the measured resistance decay. The missing power-law dependency of growing thin films is reported in literature. To overcome this problem, it was proposed by Lourens *et al.*,[12] Hoffmann *et al.*,[19] and Cheriet *et al.*[49] to divide the resistance propagation into narrow intervals of the film thickness d and to determine the percolation threshold and the conduction exponent μ by least-squares fits to these intervals. Thereby it is assumed that the χ^2 deviation rapidly decreases in the percolation region with decreasing contribution of tunneling conduction, and that the model parameters will converge to constant values. But, since d is not linearly related to p, it cannot be expected that the power-law dependence will hold

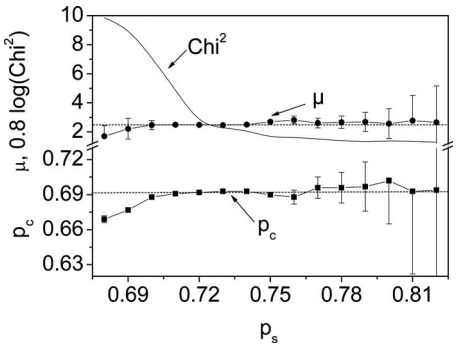

FIG. 10. Percolation threshold p_c and conduction exponent μ for Pd on sapphire, determined by least-squares fits (χ^2) of the expected power-law dependence to intervals $\Delta p=0.01$ of the surface coverage, starting at p_s. The extracted parameters are marked by dotted lines.

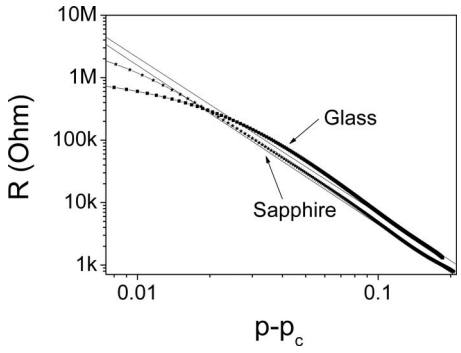

FIG. 11. Comparison of the measured resistance development and the determined power law for Pd on sapphire and glass. The resistance data are represented by a power law up to 3 orders of magnitude (sapphire), but there are deviations occurring in the vicinity of the percolation threshold.

for d as well, as it is conventionally done in literature. Therefore, in the present work the calculations have been carried out for p intervals, choosing widths $\Delta p=0.01$.

The resulting values for p_c and μ as well as χ^2 for intervals starting at p_s are plotted in Fig. 10 for Pd on sapphire as an example. As expected, the χ^2 deviation (continuous line) decreases in the percolation region, and the model parameters converge to constant values. The extracted values of $p_c=0.69\pm0.1$ and $\mu=2.55\pm0.23$ are marked by dotted lines and summarized in Table II, also for the other substrates. In Fig. 11 the comparison between the measured resistance propagation (points) and the determined power-law dependence (straight lines) is shown for Pd on sapphire and glass in a double-logarithmic plot over $p-p_c$. It can be seen that in the region where the parameters converge, the data points are represented by the power law for about 3 orders of magnitude (sapphire) of the resistance $R(p)$, in contrast to the data evaluated in literature in terms of the film thickness d, where the fit holds for only 1–2 orders of magnitude.[12,19,49] On the other hand there are occurring deviations in the direct vicinity of the percolation threshold, located on the left side of Fig. 11. Further, the power-law dependence for Pd on glass is weaker than on sapphire.

D. Continuous film conduction

Evolving from percolation the film morphology becomes more and more continuous. The onset of continuous film conduction can be determined by fitting Eq. (11) to the measured data in film thickness intervals Δd, and by plotting the difference between the measured data points and the theory.[12,19,49] When continuous film conduction applies dominantly to the film resistance, this difference should vanish. This is shown in the resulting plots in Fig. 12, where the differences rapidly vanish on an interval from nominal film thicknesses of 1.0–1.8 nm, depending on the substrate. Therefore all the film morphologies become continuous for nominal film thicknesses between 1.4 and 1.8 nm. For the mathematical treatment, the fitting intervals Δd have been chosen as $\Delta d=0.1$ nm, and in Eq. (11) $R=\rho(L/bd)$ has been applied. In Table III the starting thicknesses d_s, the minimal continuous film thicknesses $d_{\min}$, and other fitting parameters are given. Those describe the scattering of electrons at phonons and defects (ρ_0), at grain boundaries ($Z\Lambda$), and at the surface roughness with the roughness amplitude Θ. For the calculations $L=6$ mm, $b=2$ mm, and $l_0(RT)=25$ nm (Ref. 9) were applied.

TABLE II. Percolation thresholds p_c and conduction exponents μ determined for Pd on silicon, sapphire, glass, and PC by least-squares fits.

	Silicon	Sapphire	Glass	PC
p_c	0.70 ± 0.02	0.69 ± 0.01	0.715 ± 0.01	0.71 ± 0.01
μ	2.35 ± 0.35	2.55 ± 0.23	2.50 ± 0.20	2.31 ± 0.20

V. DISCUSSION

In this section all different model parameters determined in Sec. IV will be examined and correlated with each other, taking special account of their physical meaning and their consistency.

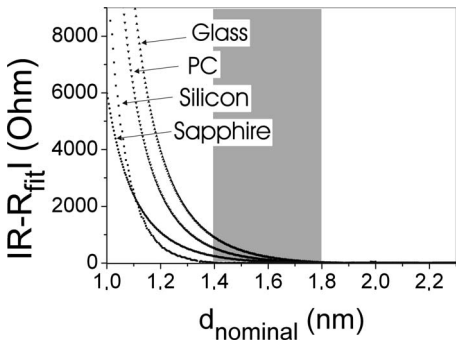

FIG. 12. Comparison of the measured film resistances and the fitted approximations by Eq. (11). Starting from the thickness value at which the differences between measured and expected resistances vanish, the growing thin Pd films can be considered as continuous. The shaded region marks the thickness interval where the Pd films on different substrates become continuous.

TABLE III. The model parameters determined for continuous Pd films in the present work compared to values calculated from the data given by Cheriet *et al.* (Ref. 49) for Ni on glass. The parameter $d_{\min}$ represents the minimal thickness of a continuous film, in which the electrical resistance is dominated by phonons and lattice defects (contribution ρ_0) as well as grain boundaries acting as Z scattering centers with mean cross section Λ and the surface roughness with roughness amplitude Θ.

Substrate	d_s (nm)	$d_{\min}$ (nm)	ρ_0 (Ω nm)	$Z\Lambda$ (nm^2)	Θ (nm)
Silicon	1.40	1.40	214.9 ± 57.9	0.147 ± 0.040	0.83 ± 0.46
Glass	1.80	1.75	250.6 ± 45.6	0.071 ± 0.026	2.25 ± 1027
PC	1.80	1.70	247.9 ± 46.1	0.079 ± 0.027	2.38 ± 1.29
Sapphire	1.80	1.60	213.0 ± 18.4	0.054 ± 0.005	1.63 ± 0.77
Ni/glass (Ref. 49)		3.8	282.6	0.60	10.17

A. Film morphologies

The initial stages of Pd films reveal an islandlike growth on glass, sapphire, and Si substrates, as shown by SEM analyses. For Pd on PC this could not be verified directly due to charging effects. But estimations can be made by regarding the work of adhesion of the system, which mainly determines the Pd growth mode on a substrate. For the Pd-PC system, a weak work of adhesion of only $W_{\mathrm{ad}}^{\mathrm{PC}}=0.8$ J/m^2 (Ref. 50) was reported. Thus, for this system islandlike growth is expected as well. For the Pd-sapphire system Hansen *et al.*[51] reported $W_{\mathrm{ad}}^{\mathrm{sapphire}}=(2.8 \pm 0.2)$ J/m^2, while for the other systems W_{ad} is unknown. Considering the low surface energy of glass ($\gamma_{\mathrm{surf}}^{\mathrm{glass}}=0.3$ J/m^2) compared to $\gamma_{\mathrm{surf}}^{\mathrm{sapphire}}=2.65$ J/m^2, $\gamma_{\mathrm{surf}}^{\mathrm{silicon}}=2.22$ J/m^2, and $\gamma_{\mathrm{surf}}^{\mathrm{PC}}=0.032$ J/m^2,[52] it is surprising that the lateral extension of the growth islands on glass is largest in each stage of growth. Otherwise it is expected that they are smallest on PC, as for lower surface adhesion energies the height-to-diameter ratio of the islands will increase and the height is assumed to be comparable for all substrates.

All growth islands show an elliptical morphology. The relations of the half axes a, b, and c determined for Pd islands on silicon by STM are in excellent agreement with the values reported by Hansen *et al.*[51] for Pd clusters with diameters larger than 5.5 nm. They reported a height-to-diameter ratio of $h/d=0.18 \pm 0.03$, comparable to $c/a=0.19 \pm 0.07$ and $c/b=0.22 \pm 0.06$ found in the present study. Since the coverage is similar for all types of substrates, it was concluded that the vertical extension also resembles that of the Si substrate.

B. Conduction between isolated islands

The upper limits of the applicability of the tunneling mechanism in growing Pd thin films, listed in Table I, are similar for the investigated substrates silicon, sapphire, and glass, reaching almost $d_{\mathrm{tunnel}}=0.70 \pm 0.03$ nm and $p_{\mathrm{tunnel}}=0.68 \pm 0.01$. The determined dielectric constants ε_r of the Pd-substrate systems for silicon and sapphire are in the upper region of the interval expected for the substrate dielectric constants $\varepsilon_{\mathrm{sub}}$. A possible reason for this effect, regarding the influence of polarized Pd islands on the dielectricities of the systems, will be explained later on when discussing the conduction model of Dryer *et al.*[36] and Leaver.[35]

The activation energies E_a for tunneling, as they are plotted in Fig. 8, lie in the range of 50–100 meV. However, the activation energy is largest for the sapphire substrate in the whole range of Pd-film growth and smallest for the silicon substrate, which leads to the conclusion that the energies are strongly determined by the electronic properties of the substrates next to the islands. This conclusion is affirmed by the mixing parameters $1-m$ as well, representing the contribution of substrate assisted tunneling to the tunneling mechanism; see Eq. (4) and Table I. On silicon the substrate contribution to the tunneling mechanism reaches 89%–100%, depending on the chosen $\varepsilon_{\mathrm{sub}}$. On glass, similar values have been found, most probably resulting from the fact that in both systems Pd is in contact with silicon oxide at the substrate surface. On sapphire, a maximum fraction of substrate assisted tunneling reaching 79% has been found. This observation of a larger contribution of vacuum tunneling is in accordance with the finding that on sapphire the steep decrease in the measured resistance with Pd-film growth, shown in Fig. 3, starts at a nominal film thickness which is almost 0.2 nm larger than for the other substrates. This directs to a reduced tunneling barrier width Δ of almost 15%. As a conclusion, the semiconductor Si seemingly favors substrate assisted tunneling.

These results can be compared to parameters recently published for palladium[23] and for other metal films. We note that in the present work the dependency of the activation energies has been directly linked to the film growth, while it is conventionally derived from temperature series for certain states of growth in other reports. Following Hill,[10] who gave a classification of discontinuous films regarding the mean island sizes and the island distances, different film results can be compared. According to the notation of Hill,[10] the films investigated in the present work are type-I films with small islands and small island separations. A list of exemplary literature data for some other type-I films has been gathered in Table IV. These can be compared to the results for the (type-I) Pd films calculated for nominal thicknesses $d_{\mathrm{nom}}=0.67$ nm.

Good agreement in the magnitude of the activation energies E_a determined in the present work is achieved with literature data on different metals. The activation energies E_a for tunneling of all different type-I films typically lie in the

TABLE IV. Comparison between the model parameters for thermally activated tunneling obtained in the present work and those taken from literature. The compared parameters are the activation energies E_a of tunneling and the mixing parameters $1-m$.

Metal	Substrate	d (nm)	r (nm)	Δ (nm)	E_a (eV)	$1-m$	Reference
Au	Na-glass		5	4	0.087		Ref. 10
Au	Na-glass		6	4	0.038		Ref. 10
Pt	Na-glass		5	2	0.0314		Ref. 10
Pt	Na-glass		7.5	2.5	0.013		Ref. 10
Pt	Glass		0.75	2.5	0.113		Ref. 10
Pt (a)	Quartz glass		0.75	8.3	0.24	1	Ref. 5
Pt (b)	Quartz glass		1.81	6.84	0.10	0.5	Ref. 5
Pt					0.0537		Ref. 30
Pt	Sapphire	0.30			0.040		Ref. 16
Ni					0.156		Ref. 30
Au					0.0403		Ref. 30
Pd	Si_3N_4		1.75	1–2	0.025		Ref. 23
Pd	$Si(O_2)$	0.67	2.75	1.41	0.041	1–0.89	This work
Pd	Glass	0.67	3.28	2.27	0.049	1–0.91	This work
Pd	Sapphire	0.67	2.51	1.71	0.061	0.79–0.62	This work

range of 10–90 meV. Mixing parameters m were reported only by Dobierzewska-Mozryzymas *et al.*[5] Further, Dobierzewska-Mozryzymas *et al.* reported just estimated data. However, the mixing parameters found in the present work can be discussed with respect to the theoretical calculations of Hill[10] and experimental data of Barwinski and Lewowski.[53] Barwinski and Lewowski investigated the influence of thin NaCl overlayers on the electrical transport in discontinuous Ag and Pt films and did not find significant effects in the activation energy of tunneling, suggesting a dominant electron transport through the substrate. This is in accordance with the contributions found in the present work.

Evaluating the tunneling current contributions of substrate assisted tunneling J_s and vacuum tunneling J_f leads to $\ln(J_s/J_f) \sim (4\pi/h)\sqrt{2m_e}(\Delta_s\sqrt{\chi}-\Delta_f\sqrt{\bar{\phi}})+(E_a^f-E_a^s)/k_BT$,[10] with the work function χ of the metal, the reduced barrier height $\bar{\phi}$, and the activation energies of substrate assisted tunneling, E_a^s, and vacuum tunneling, E_a^f. With $m_e=0.41m_0$, $\Delta_s \approx \Delta_f = 1.5$ nm, $\chi=4.45$ eV, and $\bar{\phi}=0.56$ eV (Ref. 10) for the Pd films investigated in the present work, it follows that $J_s/J_f \sim \exp[13.4+(E_a^f-E_a^s)/k_BT]$. This points out the dominance of substrate assisted tunneling for energetic reasons, supporting the strong substrate contribution to tunneling as it was determined from our measurements.

On the contrary, Dobierzewska-Mozryzymas *et al.*[5] calculated activation energies of $E_a^{(a)}=0.35$ eV and $E_a^{(b)}=0.21$ eV from the island geometry in the spherical capacitor model, setting the geometry factor as $K=4$. Besides the assumed mixing parameter of $m=0.5$, these results are critical, as the Pt films for morphological analyses have been grown on Cu grids, while the resistance measurements have been carried out on quartz glass. As shown in the present work, the film morphologies are substrate dependent, weakening the comparability of the data of Dobierzewska-Mozryzymas *et al.*[5] Questionable in this context are the results of Kazmerski and Racine,[21] who examined the electrical properties of discontinuous Au films on glass. Taking into account the given film morphologies and assuming geometry factors of $K=8$ or $K=4$ in the spherical capacitor model applied there, the given activation energies can be verified. From the results of Kazmerski and Racine,[21] it follows that $\varepsilon_r=0.18$ or $\varepsilon_r=0.36$. This is smaller than the vacuum dielectricity, and therefore the consistency of the given data is problematic. Here the necessity of the examination of all model parameters, applying for the model of thermal activated tunneling, arises. Otherwise, conflicting results might occur.

In the theoretical part of this work, conceptual uncertainties regarding the nature of the activation energy E_a and the dielectric constant ε_r of the metal-substrate system have been explained referring to the work of Dryer *et al.*[36] and Leaver.[35] As pointed out, the activation energy is assumed to be a sum of the activation energies of charge creation, $E_a^{e'}$, and charge transport, E_a^t, as given by Eqs. (8) and (9). The applicability of this model is difficult, as both energy contributions cannot be determined separately from each other, denying a direct evaluation of the measured data, as it has been carried out for the simple model of Neugebauer and Webb[30] and Hill.[10] For the calculation of the energy contributions, some assumptions on the model parameters have to be made. An approximation for the mean distance R of charge carriers in the model of Dryer *et al.*[36] and Leaver[35] is given by $\ln[(R^2/R_0^2)-2]=(E_a^e/k_BT)[1-(\alpha r/R)]$,[35] resulting in $R_{\min}=\sqrt{2}R_0$, with the mean separation $R_0=2r+\Delta$ of island midpoints. The Madelung constant is assumed to be $\alpha=1.6$, regarding two-dimensional face-centered lattices.[35] Furthermore, $\varepsilon_r^{\text{acus}}$ and $\varepsilon_r^{\text{opt}}$ have to be examined. Thereby the minimum of $E_a^{e'}$ and the maximum of E_a^t can be estimated assum-

TABLE V. Comparison of the model parameters determined with the model of Hill (Ref. 10) and the model of Dryer *et al.* (Ref. 36) and Leaver (Ref. 35) for $d_{\mathrm{nom}}=0.67$ nm. Considering the mean islands' size and distance distribution (see text) the model of Dryer *et al.* and Leaver appears to be consistent and $E_a^{\mathrm{Hill}}=E_a^{e'}+E_a^t$ is almost fulfilled.

	r (nm)	σ_r (nm)	Δ (nm)	σ_Δ (nm)	$E_a^{e'}$ [Eq. (13)] (eV)	E_a^t [Eq. (12)] (eV)	E_a (eV)
Silicon	2.75	0.84	1.41	0.7	0.008	0.033	0.041
Glass	3.28	0.26	2.27	0.6	0.013	0.042	0.049
Sapphire	2.51	0.33	1.71	0.6	0.011	0.042	0.061

ing the maximum values of the dielectric constants. In total it is expected that $E_a=E_a^{e'}+E_a^t$.

Note that in a configuration of growth islands containing charged islands, these values are increased due to the polarization of adjacent islands. Leaver[35] proved that $\varepsilon_r^i=(1-\gamma S)^{-1}\varepsilon_r^{i_0}$, with the parameter γ representing the island geometry and the structure sum S of the film. For relations 3:1 of the lateral and the vertical half axes of the growth islands, as they are almost given in the Pd islands in the present study, it follows that $\varepsilon_r^i=2.70\varepsilon_r^{i_0}$. Further we set $\varepsilon_r^{\mathrm{opt}_0}=2.5$ (Ref. 36) and $\varepsilon_r^{\mathrm{acus}_0}=$"$\varepsilon_{\mathrm{sub}}$" in Table I.

Leaver[35] pointed out that the activation energies depend on the distributions of island sizes and island distances, modifying Eqs. (8) and (9) with the standard deviations σ_i of the distributions. In this work, we further modified the prefactor with the geometric constants K as well, yielding

$$E_a^t=\frac{e^2}{K\pi\varepsilon_0}\left(\frac{1}{\varepsilon_r^{\mathrm{opt}}}-\frac{1}{\varepsilon_r^{\mathrm{acus}}}\right)\left(\frac{1}{r_4}-\frac{1}{2r_4+\Delta_1}\right) \tag{12}$$

and

$$E_a^{e'}=\frac{e^2}{K\pi\varepsilon_0\varepsilon_r^{\mathrm{acus}}}\left(\frac{1}{r_4}-\frac{\alpha}{R}\right)=E_a^e\left(1-\frac{\alpha r_4}{R}\right), \tag{13}$$

with $r_4=r+1.27\sigma_r$ and $\Delta_1=\Delta-1.27\sigma_\Delta$. Applying these equations to the Pd films, the energy contributions are calculated, as summarized in Table V. Regarding the approximations made, the relation $E_a=E_a^{e'}+E_a^t$ is almost fulfilled.

The remarkable outcome of this analysis is the observation that the energy contributions due to polarization effects are equal to those of charge creation, being the only contribution discussed in the model of Neugebauer and Webb[30] and Hill.[10] Furthermore it turns out that the high dielectric constants determined for the Pd-substrate systems probably are resulting from polarization effects.

We make one last remark regarding the initial stages of growth: Especially in the case of glass and PC substrates in Fig. 5, it unexpectedly appeared that the measured sample resistances initially after starting the deposition of Pd increased and then decreased in a wide step prior to a continuously further decay, which has been ascribed to tunneling and percolation mechanisms. A possible reason for the initial resistance propagation may be found in the metal character of the Pd growth islands themselves. Regarding the boundary conditions, the electronic states in small metallic particles are divided into discrete energy levels. Due to the reduced size, the energy gap between the Fermi level and the first excited state rapidly increases, reaching the order of 1 eV for diameters $d<2$ nm, turning the Pd islands to insulators in the initial state of growth. Therefore, the initially increasing resistance may be ascribed to an increase in the substrate roughness due to the deposition of nonconducting Pd particles. The wide step of resistance decay on the other hand may be ascribed to an insulator-metal transition of the Pd islands themselves, enabling tunneling conduction.

C. Percolation conduction

Comparing the mean percolation thresholds p_c of Pd films deposited onto silicon, sapphire, glass, and PC substrates, summarized in Table II, to the upper limit of the tunneling region of conduction, slight differences appear. In average $p_c=0.70\pm0.01$ and $p_{\mathrm{tunnel}}\leq0.68\pm0.01$. The reasons for these slight deviations are assumed to result from the interference of both conduction mechanisms near the percolation threshold, resulting in an increasing curvature of the resistance decay plotted in Fig. 11, while with the absence of tunneling conduction at the percolation threshold a sharp resistance drop would be expected.

Considering the power-law parameters (Table II), for p_c excellent agreement with $p_c^{\mathrm{theor}}=0.688$ (Ref. 41) is achieved, allocating a two-dimensional growth mode of the discontinuous Pd films at room temperature. But remarkable deviations from the expected conduction exponent $\mu^{\mathrm{theor}}=1.3$ (Ref. 14) and the measured values are apparent, which are equal for the different investigated substrates within the error bars and amount to $\mu=2.43\pm0.12$ in average. This value is larger than that expected for three-dimensional continuous percolation as well. The equality of the measured values thereby underlines their significance, manifesting that they are linked to physical effects beyond the percolation model. Possible reasons for the deviations might be found in the morphology of the percolating Pd films, the additional mechanism of island coalescence, and electronic effects of the Pd-substrate systems, which shall be proposed as follows.

A morphological effect, weakening the percolation transition and thereby changing the model parameters, can be assumed in the distribution of island sizes and the islands' separations in the discontinuous films, preventing the existence of a sharp percolation threshold. Furthermore, a basic difference between a percolating metal film and the theoretical model systems of two-dimensional percolation is found

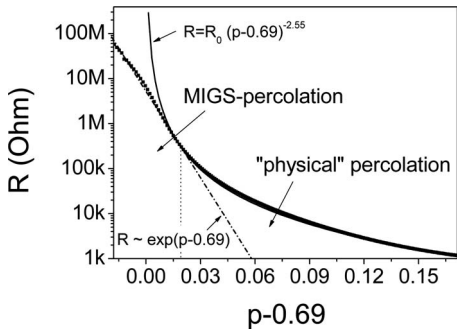

FIG. 13. In the direct vicinity of the percolation threshold the resistance development of Pd growing on sapphire exhibits an exponential decay. This supports the existence of a MIGS percolation, induced by the overlapping of the MIGS created by adjacent islands, prior to the islands getting into physical contact themselves.

on the atomistic scale. During coalescence, caused by adatom diffusion between two coalescing clusters, a rapidly growing neck is formed, accelerating the formation of a larger cluster. Thereby the two adjacent clusters merge, in contrast to a theoretical model of percolating hard spheres. The neck formation, rapidly increasing the conducting area between the clusters, might cause an increased conduction exponent.

But in Fig. 11 deviations of the measured resistance from the expected resistance dependency occurred in the vicinity of the percolation threshold. A possible reason for this effect might be found in an increase in the electronic partition sum of the substrate close to the interface to the metal clusters, caused by the formation of metal induced gap states (MIGSs).[54,55] If the lateral distance between two adjacent metal clusters is small, it may be assumed that the MIGSs induced by both clusters overlap prior to the clusters getting into physical contact themselves. Therefore, prior physical percolation a mechanism of gap state percolation may be proposed, shown in Fig. 13 for Pd on sapphire. As the MIGS range decreases exponentially in the vicinity of a cluster, due to gap state percolation not a power-law dependence but an exponential decrease in the resistance would result, clearly present in the resistance dependency of Pd on sapphire near p_c.

This argument is assisted by the observation of increasing deviations between the measured and the expected resistance dependencies in the order of Pd on sapphire, glass, and silicon. The reason may be found in the different band-gap widths of the different substrates.

In literature a wide variation of different techniques is applied in investigating the percolation conduction of metal films. As listed in Table VI, different methods result in different percolation parameters, underlining the nonuniversality of the physical properties of percolating systems. Interestingly, the percolation thresholds determined in Refs. 57 and 58 are closer to the one expected for two-dimensional bond percolation, $p_c=0.5$,[37] than that of continuous percolation. For the deposition of Co clusters of varying size, Yamamuro *et al.*[56] found different percolation exponents, explained based on cluster size dependent diffusion rates on the substrate surface. Taking the variety of conduction exponents into account, the values reported in the present work do not oppose those reported earlier. They increase the range of possible conduction exponents, also with respect to the given explanations. Further, the mechanisms discussed in this work might contribute to the electrical conductivity of the other films as well.

D. Continuous film conduction

All investigated Pd films exhibit similar resistivities when they become continuous. Taking the Pd bulk value $\rho_0^{\text{bulk}}=108\ \Omega$ nm (Ref. 9) into account, the magnitude of the calculated values is also confirmed. They are larger than the bulk value, as the morphology of a continuous film with $d_{\text{nom}}=2$ nm is not closed but contains numerous holes and

TABLE VI. Comparison of the percolation thresholds p_c and conduction exponents μ determined for percolating Pd films in the present study and representative literature data.

System	Preparation method	$T(K)$	p_c	μ	Reference
Ag/SiO_2	Annealing agglomeration	908		1.25 ± 0.1	Ref. 14
Co/SiO_2	Cluster deposition, $d_{\text{Clu}}=6-13$ nm		0.63	1.1–1.8	Ref. 56
	Stamping holes into a sheet		0.63–0.55	1.78–1.80	Ref. 18
Ni/glass	Thermal evaporation	300	0.39	2	Ref. 57
Ni/glass		295		1.27 ± 0.1	Ref. 49
Cr/glass		658		1.34 ± 0.11	Ref. 12
Al/NaCl	Thermal evaporation	373	0.51	1.9	Ref. 58
Al/NaCl	Thermal evaporation	423	0.51	2.3	Ref. 58
W	Annealing agglomeration of W-sapphire-cermets (3D)	1500	0.47 ± 0.05	1.9	Ref. 31
Pd/sapphire	Sputter deposition	300	0.69 ± 0.01	2.55 ± 0.23	This work
$Pd/Si(O_2)$	Sputter deposition	300	0.70 ± 0.02	2.35 ± 0.35	This work
Pd/PC	Sputter deposition	300	0.71 ± 0.01	2.31 ± 0.20	This work
Pd/glass	Sputter deposition	300	0.715 ± 0.01	2.50 ± 0.20	This work

structural defects. The tendency of the products $Z\Lambda$ determined for the different substrates appears questionable. As it is a measure of the number of grain boundaries in the film, it should decrease with increasing grain size. Therefore the value for the PC substrate should be the largest. The calculated roughness amplitudes Θ are larger than the nominal film thicknesses for all substrates except silicon, while the tendency of a decreasing roughness with increasing grain size is almost represented. Therefore, regarding the inconsistencies, the physical significance of the model of Finzel and Wissmann[47] for the investigated films is questionable in detail. It seems as if more contributions have to be taken into account to consistently model the continuous film conduction regime. For comparison, the values calculated from the model parameters given by Cheriet *et al.*[49] for Ni on glass with $l_0^{\mathrm{Ni}}=18$ nm (Ref. 9) are listed in Table III as well.

VI. SUMMARY

In the present study the conduction mechanisms in growing discontinuous Pd films on different substrates were investigated in detail, including the regimes of thermally activated tunneling, percolation conduction, and continuous film conduction. The aim of this work was to give a consistent description of the conductivity of a growing Pd film where the different model parameters are in accordance with each other. The different conduction regimes can be separated but they strongly interfere. No sharp percolation threshold can be observed, but percolation is superimposed by tunneling conduction, morphological changes in the films, and MIGS contributions.

The existing models of thermally activated tunneling between isolated islands[10,30] were modified subsequently by the introduction of the geometry factor K. Besides this, model parameters such as the dielectric constants ε_r of the Pd-substrate systems and the activation energies E_a of tunneling were determined. The activation energies lie on the order of 50 meV. A large substrate contribution to the tunneling mechanism has been deduced and comparable contributions of charge creation and charge transfer to the tunneling process were found. Regarding percolation conduction, uncertainties in the direct vicinity of the percolation thresholds were observed, as the resistance decays exponentially there. This effect was explained by establishing the idea of a metal induced gap state percolation, occurring prior to the physical percolation of the growth islands. The determined percolation thresholds of $p_c=0.70$ fit well to the model of two-dimensional continuous percolation, while the observed conduction exponents of $\bar{\mu}=2.43$ are very large. This is explained based on the morphological properties of the percolating films. Continuous film conduction was described in terms of the model of Finzel and Wissmann.[47] Thereby the minimal film thicknesses of continuous RT-sputtered Pd films was found to be on the order of 1.5 nm. Further model parameters such as the resistivity of the growing films appeared to be in accordance with the theoretical expectations, while other model parameters such as the number of scattering centers do not evolve intuitively.

All contributions to the conduction mechanisms only come into sight because the different regimes were regarded in total. Therefore, this work might stimulate the discussion of different regimes of other metals in its complexity. Further, the gained knowledge on the electrical properties of growing Pd thin films can count as a basis of further investigations in fundamental research and in the field of sensor applications.

[1] M. Idrish Miah, J. Phys. D **41**, 035105 (2008).
[2] A. Sawa, T. Fujii, M. Kawasaki, and Y. Tokura, Appl. Phys. Lett. **88**, 232112 (2006).
[3] A. M. Haghiri-Gosnet and J. P. Renard, J. Phys. D **36**, R127 (2003).
[4] H. Graf, J. Vancea, and H. Hoffmann, Appl. Phys. Lett. **80**, 1264 (2002).
[5] E. Dobierzewska-Mozrzymas, E. Pieciul, and P. Bieganski, Cryst. Res. Technol. **36**, 1137 (2001).
[6] C. Pennetta, L. Reggiani, and G. Trefan, Phys. Rev. Lett. **84**, 5006 (2000).
[7] H. Nakashima and K. Uozumi, Thin Solid Films **281-282**, 383 (1996).
[8] G. X. Ye, Y. Q. Xu, J. S. Wang, Z. K. Jiao, and Q. R. Zhang, Phys. Rev. B **49**, 3020 (1994).
[9] M. Angadi, J. Mater. Sci. **20**, 761 (1985).
[10] R. Hill, Proc. R. Soc. London, Ser. A **309**, 377 (1969).
[11] V. Loboda and S. Khursenko, J. Exp. Theor. Phys. **103**, 790 (2006).
[12] J. A. J. Lourens, S. Arajs, H. F. Helbig, L. Cheriet, and El-Sayed A. Mehanna, J. Appl. Phys. **63**, 4282 (1988).
[13] A. Boltaev, N. Penin, A. Pogosov, and F. Pudonin, J. Exp. Theor. Phys. **99**, 827 (2004).
[14] K. Sieradzki, K. Bailey, and T. Alford, Appl. Phys. Lett. **79**, 3401 (2001).
[15] S. T. Ruggiero, T. B. Ekkens, and S. Farhangfar, Phys. Rev. B **63**, 195405 (2001).
[16] I. Ostadal and R. M. Hill, Phys. Rev. B **64**, 033404 (2001).
[17] A. Bishay, W. Fikry, and H. Hunter, J. Phys. D **33**, 2218 (2000).
[18] A. Okazaki, K. Horibe, K. Maruyama, and S. Miyazima, Phys. Rev. E **61**, 6215 (2000).
[19] T. Hoffmann, J. Martinez-Salazar, P. Herrero, and J. Petermann, Phys. Rev. B **55**, 1858 (1997).
[20] M. Octavio, G. Gutierrez, and J. Aponte, Phys. Rev. B **36**, 2461 (1987).
[21] L. Kazmerski and D. Racine, J. Appl. Phys. **46**, 791 (1975).
[22] O. Dankert and A. Pundt, Appl. Phys. Lett. **81**, 1618 (2002).
[23] J. van Lith, A. Lassesson, S. Brown, M. Schulze, J. Partridge, and A. Ayesh, Appl. Phys. Lett. **91**, 181910 (2007).
[24] M. Ohring, *The Materials Science of Thin Films* (Academic, New York, 1991).
[25] J. Merwe, Interface Sci. **1**, 77 (1993).
[26] G. Jeffers, M. Dubson, and P. Duxbury, J. Appl. Phys. **75**, 5016 (1994).

[27] M. Blazej and E. Dobierzewska-Mozrzymase, Thin Solid Films **192**, 219 (1990).
[28] G. Witt, Thin Solid Films **22**, 133 (1974).
[29] J. Morris and T. Coutts, Thin Solid Films **47**, 3 (1977).
[30] C. Neugebauer and M. Webb, J. Appl. Phys. **33**, 74 (1962).
[31] B. Abeles, H. Pinch, and J. Gittelmann, Phys. Rev. Lett. **35**, 247 (1975).
[32] J. Jeans, *The Mathematical Theory of Electricity and Magnetism* (Cambridge University Press, Cambridge, England, 1923).
[33] J. Simmons, J. Appl. Phys. **34**, 1793 (1963).
[34] M. Poschenrieder, Ph.D. thesis, TU Berlin, 2000.
[35] K. Leaver, J. Phys. C **10**, 249 (1977).
[36] J. Dryer, D. Gore, and R. Speiser, J. Vac. Sci. Technol. **10**, 316 (1973).
[37] A. Bunde, *Fractals and Disordered Systems* (Springer-Verlag, Berlin, 1991).
[38] J. Kertesz and T. Vicsek, Z. Phys. B: Condens. Matter **45**, 345 (1982).
[39] S. Kirkpatrick, Phys. Rev. Lett. **27**, 1722 (1971).
[40] A. Kapitulnik and G. Deutscher, Phys. Rev. Lett. **49**, 1444 (1982).
[41] T. Vicsek and J. Kertesz, J. Phys. A **14**, L31 (1981).
[42] I. Webman, J. Jortner, and M. Cohen, Phys. Rev. B **16**, 2593 (1977).
[43] E. Sondheimer, Adv. Phys. **1**, 1 (1952).
[44] I. Rahman, J. Appl. Phys. **52**, 5859 (1981).
[45] A. Mayadas and M. Shatzkes, Phys. Rev. B **1**, 1382 (1970).
[46] C. Tellier, C. Pichard, and A. Tosser, J. Phys. F: Met. Phys. **9**, 2377 (1979).
[47] H. Finzel and P. Wissmann, Ann. Phys. **43**, 5 (1986).
[48] S. Wagner, Diploma thesis, University of Göttingen, 2005.
[49] L. Cheriet, H. H. Helbig, and S. Arajs, Phys. Rev. B **39**, 9828 (1989).
[50] A. Pundt, E. Nikitin, P. Pekarski, and R. Kirchheim, Acta Math. **52**, 1579 (2004).
[51] K. H. Hansen, T. Worren, S. Stempel, E. Laegsgaard, M. Baumer, H.-J. Freund, F. Besenbacher, and I. Stensgaard, Phys. Rev. Lett. **83**, 4120 (1999).
[52] G. Song, Ph.D. thesis, University of Bochum, 2000.
[53] B. Barwinski and T. Lewowski, Thin Solid Films **61**, 141 (1979).
[54] A. Zangwill, *Physics at Surfaces* (Cambridge University Press, Cambridge, England, 1998).
[55] D. A. Muller, D. A. Shashkov, R. Benedek, L. H. Yang, J. Silcox, and D. N. Seidman, Phys. Rev. Lett. **80**, 4741 (1998).
[56] S. Yamamuro, K. Sumiyama, and T. Hihara, J. Phys.: Condens. Matter **11**, 3247 (1999).
[57] A. Maaroof and B. Evans, J. Appl. Phys. **76**, 1047 (1994).
[58] E. Dobierzewska-Mozrzymas and P. Bieganski, Surf. Sci. **200**, 417 (1988).